KSME

Springer

Journal of Mechanical Science and Technology 34 (1) 2020

Original Article
DOI 10.1007/s12206-019-1220-2

Keywords:
· Centrifugal pump
· Clearance flow
· Numerical simulation
· Pressure fluctuation

Correspondence to:
Lulu Zheng
zhengll012@163.com

Citation:
Zheng, L., Chen, X., Dou, H.-S., Zhang, W., Zhu, Z., Cheng, X. (2020). Effects of clearance flow on the characteristics of centrifugal pump under low flow rate. Journal of Mechanical Science and Technology 34 (1) (2020) 189-200. http://doi.org/10.1007/s12206-019-1220-2

Received May 17th, 2019
Revised August 12th, 2019
Accepted October 15th, 2019

† Recommended by Editor Yang Na

Effects of clearance flow on the characteristics of centrifugal pump under low flow rate

Lulu Zheng[1], Xiaoping Chen[2], Hua-Shu Dou[2], Wei Zhang[2], Zuchao Zhu[2] and Xueli Cheng[1]

[1]Faculty of Mechanical Engineering, Henan Institute of Technology, Xinxiang, Henan 453003, China, [2]National-Provincial Joint Engineering Laboratory for Fluid Transmission System Technology, Zhejiang Sci-Tech University, Hangzhou, Zhejiang 310018, China

Abstract The Reynolds averaged Navier-Stokes equations and the shear stress transport *k-ω* turbulence model are employed to simulate the centrifugal pump with or without clearance flows. The simulation results have been compared with the experimental data and good agreement has been achieved. Results show that clearance flow causes a decrease in the characteristics of the centrifugal pump, particularly in pressure fluctuation. The largest deviation of the amplitude of pressure fluctuation between the centrifugal pump with and without clearance flow is 65.34 %. The numerical results also show that the clearance flow causes collision impact with the mainstream flow and forms a multiple vortex structure at the impeller entrance. Clearance flow greatly affects the pressure distribution in the impeller passage, which is opposite to the volute tongue, especially at the suction side of the blade surface. The wave distribution decreases along the direction of the hub to the shroud, which indicating that the influence of clearance flow weakens along this direction.

1. Introduction

Centrifugal pumps are widely used in fluid transportation and energy conversion engineering applications, such as aeronautical and astronautical industries, ocean engineering, hydraulic engineering and the electricity and petrochemical industries [1-6]. The complex internal flow, including the main flow and clearance flow, plays a crucial role in the efficient energy conversion, operation safety, and the service life of centrifugal pumps.

A large number of studies on the internal flow of the centrifugal pumps have been carried out on the main flow, including rotor-stator interaction [7-16], separating vortex [17, 18], rotating stall [19-22], and secondary flow [23-26]. For example, strong interaction between the impeller and volute directly affect the stable operation of the pump. Thus, the intense pressure fluctuation must be reduced to improve the performance of the pump. Spence et al. [15] and Zhang et al. [16] analyzed the influence of geometrical parameters on the pressure pulsation characteristics of the pump and found that appropriate geometry can effectively reduce the pressure pulsation intensity in the pump. The rotating stall, which is an unsteady flow phenomenon in the impeller, which generally causes low frequency vibration and even damages the pump [20]. Meanwhile, secondary flow plays an important role in centrifugal pumps. Detailed studies on secondary flow were carried out through PIV measurements and numerical methods [26].

Note that all of the aforementioned studies are without including clearance flow, only focus on the flow in the impeller and volute. The clearance between the rotating impeller and stationary casing plays an important role in centrifugal pumps. However, it is normally omitted in the numerical predictions of the internal and external performance of the pump, because it greatly affects the internal flow and performance of the pump [27]. Leakage flow through the wear ring clearance causes the variation of the internal flow situation due to the clearance inside the pump, resulting in volumetric loss. Therefore, the clearance flow and its influence must be

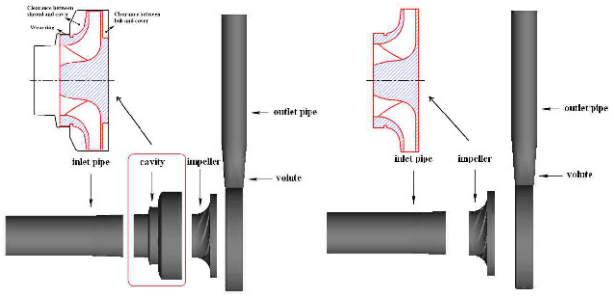

(a) Model A (b) Model B

Fig. 1. Schematic of the two centrifugal pump models.

investigated [28-33]. Liu et al. [34] investigated the characteristics of tip leakage vortex in a mixed flow pump and revealed the spatial-temporal evolution of the tip leakage vortex. Cao et al. [35] studied the effect of axial clearance on the efficiency of a shrouded centrifugal pump and found that volumetric efficiency is most sensitive to the axial clearance. The wear ring clearance is an important part of the leakage flow path of the pump and the wear ring clearance flow greatly affect the head and total efficiency of the centrifugal pump [36]. In addition, the variable of the clearance of front wear ring has the most influence on the performance of a centrifugal pump [37, 38]. In recent years, DaqiqShirazi et al. [39] studied the effect of wear ring clearance on flow field in the impeller sidewall gap and the variation of the efficiency in a low specific speed centrifugal pump. Yan et al. [40] numerically analyzed the effect of flat ring seal and labyrinth seal on the leakage and efficiency of a pump-turbine with 0.2 mm and 0.5 mm wear ring clearance. They found that the impact of the leakage flow is very large and cannot be ignored.

The effect of clearance flow on characteristics of centrifugal pump is still not fully understood due to the limited research linked to clearance flow within the centrifugal pump. Furthermore, the effect of clearance flow on streamline distribution at the impeller entrance and pressure distribution within the centrifugal pump must be examined in detail, especially at low flow rate. Therefore, studying the influence of clearance flow on the characteristics of centrifugal pumps under low flow rate is an urgent research undertaking.

The main objective of the present study is to investigate the influence of clearance flow on the characteristics of the centrifugal pump under low flow rate. The structure is organized as follows. The model description and numerical methods are discussed in Sec. 2. Sec. 3 presents the results and discussions. Finally, we summarize our findings in Sec. 4.

2. Model description and numerical methods

2.1 Physical models

Fig. 1(a) shows the centrifugal pump model, which is named as model A, it is consists of the cavity, impeller, volute, inlet, and outlet pipe. The cavity includes the clearance region between the rotating impeller and the stationary casing. The performance and geometric parameters of model A are listed in Table 1. To clarify the effect of clearance flow on the characteristics of the centrifugal pump, a centrifugal pump model without clearance flow was also developed and named as model B, as shown in Fig. 1(b).

Table 1. Performance and geometric parameters.

Parameters	Sign	Value
Flow rate (m^3/h)	Q_d	45
Head (m)	H_d	30.9
Efficiency (%)	η	64.5
Rotation speed (r/min)	n_d	2900
Specific speed	n_s	90
Blade number	Z	6
Wear ring clearance (mm)	b	0.35
Wear ring clearance length (mm)	l	13
Impeller inlet diameter (mm)	D_1	86
Impeller outlet diameter (mm)	D_2	161

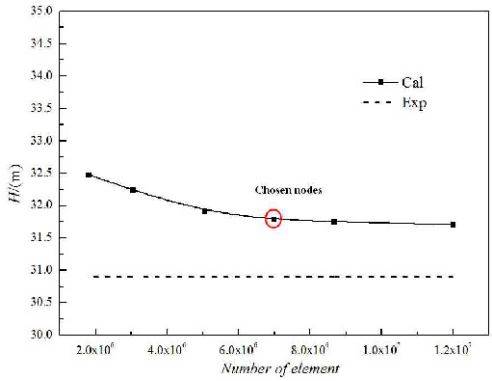

Fig. 2. Mesh independency validation.

2.2 Numerical methods

The governing equations used were the unsteady three-dimensional incompressible Reynolds-averaged Navier-Stokes equations. The main form of governing equations is as follows:

$$\frac{\partial u_i}{\partial x_i} = 0 \tag{1}$$

$$\frac{\partial}{\partial t}(\rho u_i) + \frac{\partial}{\partial x_j}(\rho u_i u_j) = -\frac{\partial p}{\partial x_i} + \frac{\partial}{\partial x_j}\left(\mu \frac{\partial u_i}{\partial x_j}\right) + S_i \tag{2}$$

where ρ is fluid density, x_i is the components in i direction, u_i are the average velocity components in i direction, S_i is the source term. The commercial CFD code ANSYS-Fluent was used to solve the governing equations. Turbulent flow was solved by the shear stress transport k-ω turbulence model, and

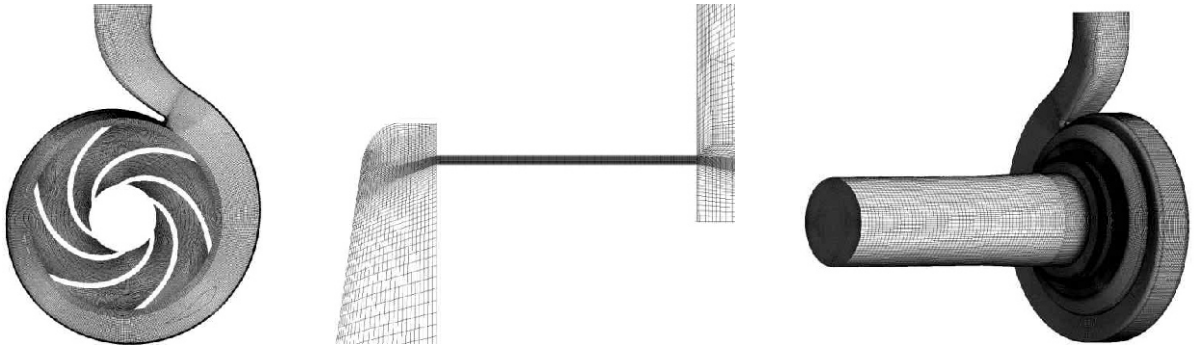

(a) Center plane (b) Wear ring (c) Centrifugal pump

Fig. 3. Mesh diagram of the centrifugal pump.

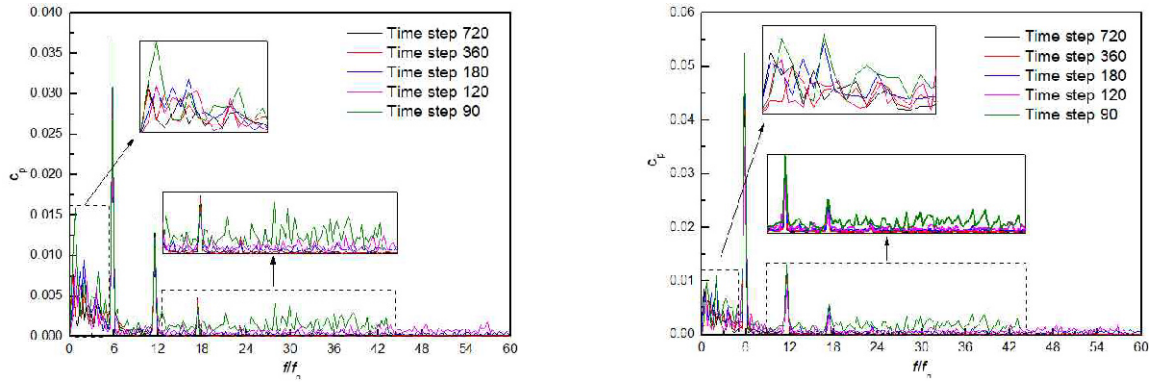

(a) Monitor point near the tongue (b) Monitor point near the volute outlet

Fig. 4. FFT results of the pressure under various time step per impeller revolution.

standard wall functions were applied in the simulation. The system was solved by the finite volume method, and the coupling between velocity and pressure was achieved by using the SIMPLE algorithm. The boundary conditions included the velocity condition at the inlet and outflow of pump outlet. The steady numerical simulation result was initially obtained using the multiple frame of reference (MRF) method. The computational data of steady flow in the centrifugal pump was taken as the initial condition of unsteady computation. The convergence criterion is set as 1×10^{-5} for both steady and transient simulations, which is enough to obtain accurate results.

Structured hexahedral mesh was generated for the computational domain of the centrifugal pump, it had better convergence characteristics during the numerical calculation. Six sets of meshed tests were conducted for model A to validate the mesh independence. The total mesh numbers are 1.81 million, 3.04 million, 5.07 million, 6.98 million, 8.68 million and 12.0 million. These mesh schemes were carried out for model A at designed flow rate. Fig. 2 shows the head of these mesh schemes. The results show that, with the increase in the mesh element, no significant difference between the results is obtained by the mesh with 6.98 million cells. This mesh size can obtain satisfactory simulation accuracy, provide accurate results for the pump performance, and allow details of the main flow pattern involved to be analyzed. Thus, the case with 6.98 million mesh numbers was selected for the final simulation. The mesh details are shown in Fig. 3. The mesh numbers in the inlet pipe, outlet pipe, pump chamber, volute, and impeller are 216732, 204533, 3819421, 1327226, and 14139118, respectively.

Time step size directly affects the temporal discretization accuracy, which is of great significance to the present work focusing on the accuracy of the clearance flow. Fig. 4 illustrates the FFT results of the pressure fluctuation with model A under various time step (TS) sizes, including 90, 120, 180, 360 and 720 time steps per impeller revolution at nominal flow rate. The blade passing frequency f_{BPF} and its harmonic frequency are captured in the frequency domain distribution. With the decrease of the time step size per impeller revolution, the pressure frequency signals show an increasing trend. Therefore, larger value of the time step size per impeller revolution is preferred in order to obtain accuracy resolution. Finally, taking the calculation accuracy and calculation resources into consideration, the time step size with 360 time steps per impeller revolution (Δt = 5.575×10^{-5} s) is selected as the unsteady calculation time step. All the numerical simulations are carried out on a HP server with 16 central processing units. It takes about 188 hrs for calculating one case.

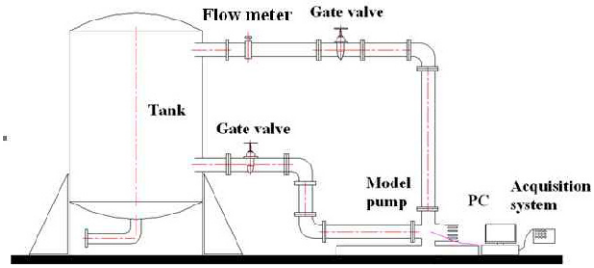

(a) Pipeline line diagram

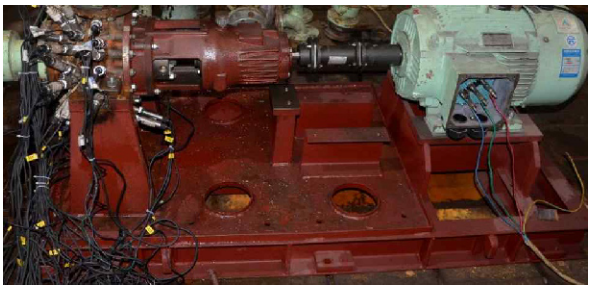

(b) Test pump

Fig. 5. Test platform.

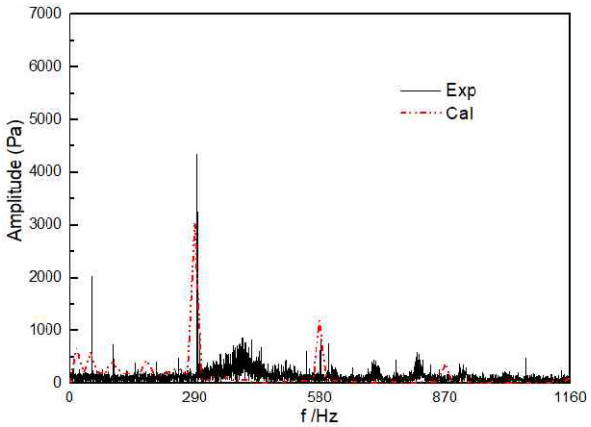

(a) Monitor point near the tongue

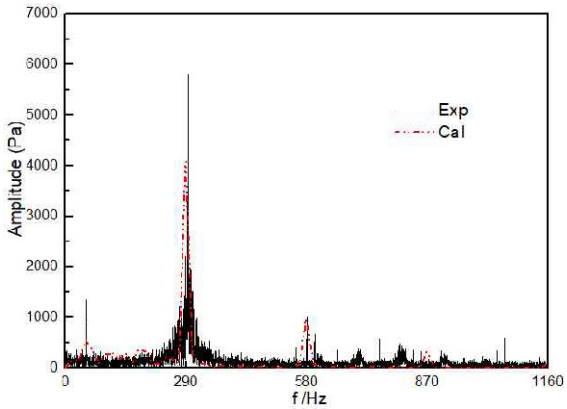

(b) Monitor point near the volute outlet

Fig. 6. Pressure fluctuation in the frequency domain under nominal flow rate.

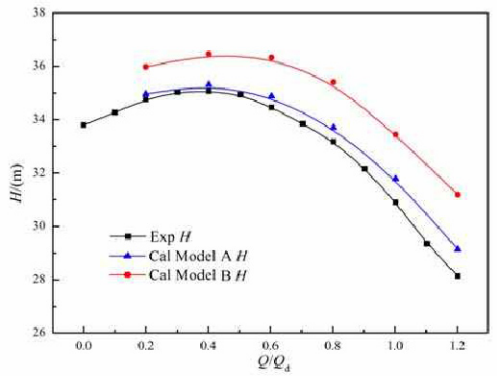

(a) Head curve

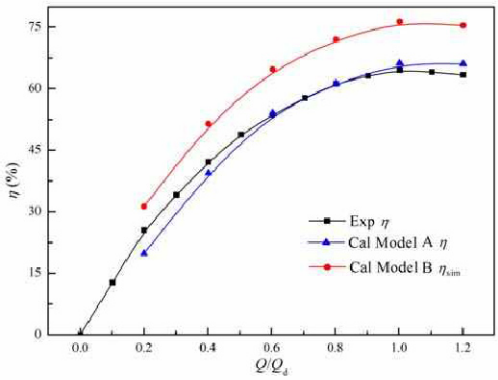

(b) Efficiency curve

Fig. 7. Comparison between the experimental and numerical results of the centrifugal pump.

2.3 Validation of the calculation results

The numerical results of model A were verified by measuring the pump performance characteristics and unsteady pressure fluctuations. The experiments of the centrifugal pump are conducted at National-Provincial Joint Engineering Laboratory for Fluid Transmission System Technology of Zhejiang Sci-Tech University. The test platform consisted of a centrifugal pump, a tank, a circulation-line system, pressure sensors, data acquisition and processing system, as shown in Fig. 5. The centrifugal pump was driven by a 7.5 kW electromotor with a variable frequency controller. The rotational speed was measured by using a photoelectric tachometer. The sensor ranges were -0.1 to 0.1 MPa and 0 to 1.0 MPa. All data signals were identified and stored in the computers for further analysis.

Figs. 6(a) and (b) respectively show the pressure fluctuation distribution in the frequency domain of the experimental results and numerical simulation with model A at nominal flow rate. The dominant frequency is observed in the numerical and experimental results. The f_{BPF} obtained by the experiment is slightly higher, because of the factors, such as motor and voltage in the actual operation.

Fig. 7 presents the comparison of experimental and numerical results of model A. Note that the numerical results show good agreement with the experimental results. In the full flow

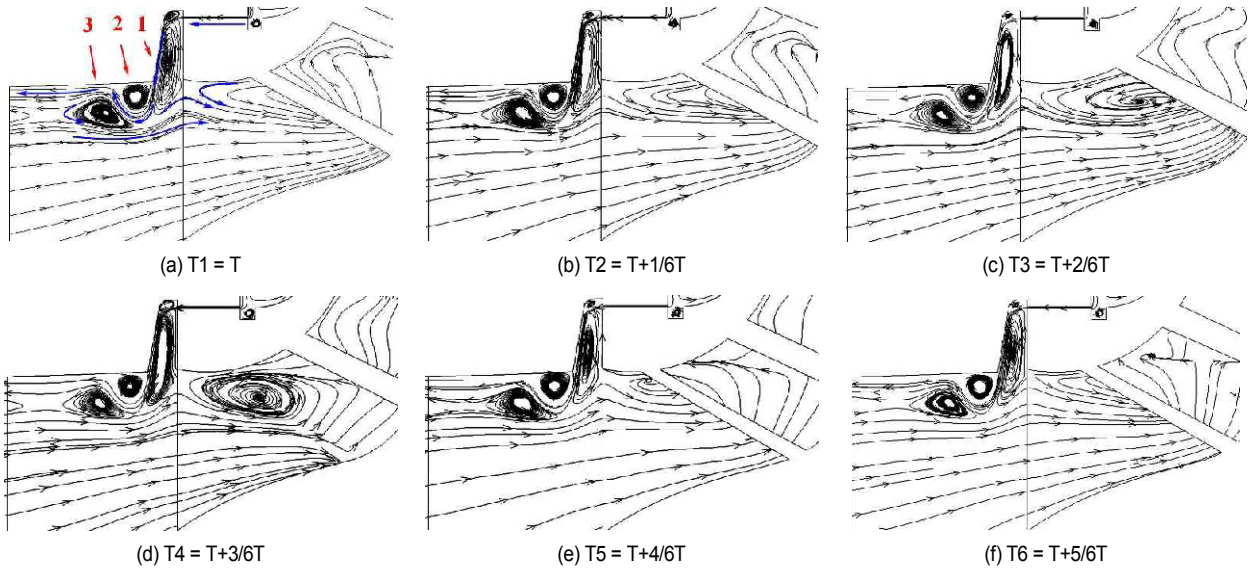

Fig. 8. Absolute velocity distribution on cross-section of model A.

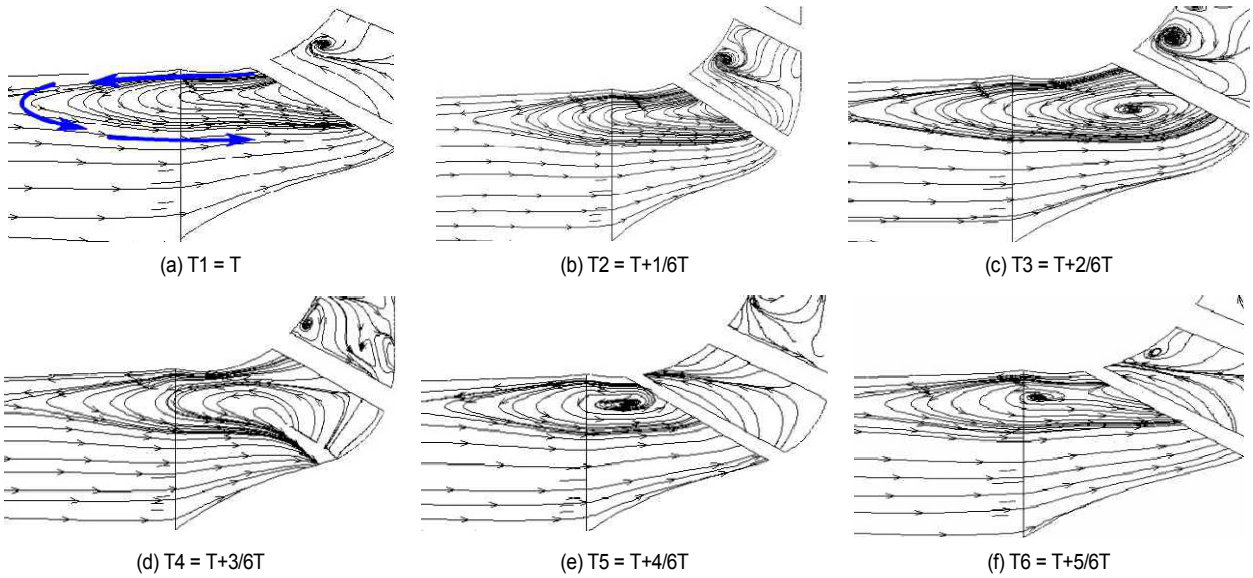

Fig. 9. Absolute velocity distribution on cross-section of model B.

range, the maximum deviation of the head curve and the efficiency curve is within 4 %, which reflects the accuracy of the numerical calculation results.

The results of model B are also shown in Fig. 7 to investigate the influence of clearance flow on the head and efficiency of the pump. The predicted results of model A and model B exhibit similar distribution tendencies. However, the numerical results of the head and efficiency of model A is evidently lower than those of model B. In comparison with model B, the head and efficiency of model A decreased by 4.37 % and 19.47 % under various flow rates on average, because model B ignores the flow loss caused by the clearance flow in the pump, finally resulting in a large difference in the head and efficiency between the two models.

In summary, the calculated external characteristics curve of model A is quite different from those of model B without considering the clearance flow. It is well known that the internal flow of centrifugal pumps is complicated, especially under partial flow rate. Detailed analysis on the characteristics of the clearance flow and its influence on the internal flow field of centrifugal pumps are of great significance under partial flow rate. Therefore, the following section is performed at $0.2Q_d$.

3. Results and discussions

3.1 Effect of clearance flow on streamline distribution of impeller entrance

Figs. 8 and 9 show the distribution of the streamline at differ-

ent flow times. The rotation period of an impeller passage is named as T, which is equal to 60 degrees in the present study. The high-energy leakage flow from the wear ring impinges on the pump casing at a high speed, and then flows along the casing towards the impeller inlet (the flow direction is presented by the blue arrow). A large vortex, which is named as vortex 1, is formed under the coaction of the shearing of the high-speed and high-energy leakage flow, as shown in Fig. 8(a). The vortex has a certain squeezing effect on the mainstream of the impeller inlet and causes the flow deviation at the impeller inlet. Subsequently, wear ring leakage flow collides with the mainstream flow of the impeller. The interaction between clearance flow and mainstream flow is basically divided into the collision impact stage, reversing mixing stage, and the assimilation stage. During the collision impact stage, the high-speed leakage flow collides with the low-speed mainstream of the impeller and results in a vortex near the surface of the pump inlet, namely vortex 2. In the reverse mixing stage, the leakage flow moves in the opposite direction of the mainstream flow and mixes with the mainstream flow. Vortex 3 is generated under the action of the mainstream and the leakage flow. In the assimilation phase, the interaction between the wear ring leakage flow and the mainstream flow results in a rapid energy loss of leakage flow. When the leakage flow energy is exhausted, it flows into the impeller along with the main flow.

The assimilated fluid and the reverse flow near the shroud flow into the impeller together. In the interaction between the leakage flow and the impeller mainstream flow, multiple vortices are generated. The vortices adjacent to each other rotate in opposite directions and are mainly distributed near the wall. With the rotation of the impeller, the multiple vortices do not change evidently. However, the influence area of reverse flow changes during the rotation period at the entrance of the impeller. For comparison, the streamline distribution of model B is presented in Fig. 9. The figure shows significant reverse flow area, which is located at the entrance of the impeller. The local fluid flows backward from the impeller inlet into the inlet pipe. The reverse flow direction and its influence range are shown by the blue arrows. This flow phenomena includes the reversing mixing stage and the assimilation stage. A large reverse flow is observed at the entrance of the impeller. With the rotation of the impeller, the reverse flow area always appeared at impeller inlet near the shroud region. No significant variation of the reverse flow area is found at the impeller inlet, whereas the center position of the vortex changes with the rotating impeller.

In summary, clearance flow greatly affects the internal flow at the entrance of the impeller. Compared with the model without clearance, the existence of clearance flow causes a new flow phenomenon, that is, the collision impact stage. In addition, clearance flow results in the multiple vortices structure found at the impeller entrance and inhibits the reverse flow at impeller entrance near the shroud region. Clearance flow causes large change of flow structure at the entrance of the impeller. Thus, the influence of the clearance flow must be considered to obtain accurate flow results of the pump.

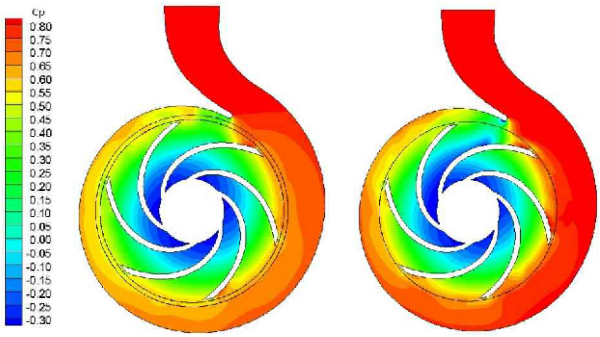

(a) Model A (b) Model B

Fig. 10. Pressure distribution on the center plane.

3.2 Effect of clearance flow on pressure distribution of the volute

The pressure coefficient is defined as follows:

$$c_p = \frac{p - p_{ref}}{0.5\rho u_2^2} \tag{3}$$

where p_{ref} is the reference pressure, and u_2 is the circumferential velocity of the impeller.

Fig. 10 shows pressure distribution on the center plane. As can be seen in the low-pressure area at the impeller inlet, the pressure increases gradually along the direction from the impeller inlet to the outlet. A similar phenomenon is observed in Refs. [41-44]. However, the difference in pressure distribution of the two models is mainly reflected in the value. In general, the pressure in the volute of model A is lower than that of model B due to the clearance flow.

The pressure fluctuation data during the last three impeller period were obtained to quantitatively analyze the influence of the clearance flow on the pressure inside the volute. Fig. 11 shows the pressure fluctuation and frequency spectra, the points position is indicated in Fig. 11(d).

The distribution of pressure at each monitoring point shows evident periodicity, which is clearly denoted in Figs. 11(a)-(c). Six peaks and valleys are found within one impeller period. A similar phenomenon is observed in Refs. [45-47]. The amplitudes of the peaks and valleys exhibit a certain difference. The comparison between the pressure fluctuation at the same monitoring point indicates the slight difference in the average pressure of the monitoring point between model A and model B. However, the pressure fluctuation amplitude is quite different. Evidently, the corresponding amplitude of the monitoring point in model A is significantly lower than that of model B, as shown in Figs. 11(a)-(c). The blade passing frequency and its multiples are found in the distribution of pressure spectra, whereas the corresponding amplitude of the f_{BPF} of each monitoring point is significantly different, as shown in Figs. 11(d)-(f). Results show that the amplitude, which corresponds to f_{BPF} from P1 to P3, decreases successively. A similar phenomenon is observed in Ref. [48]. The existence of the clearance flow

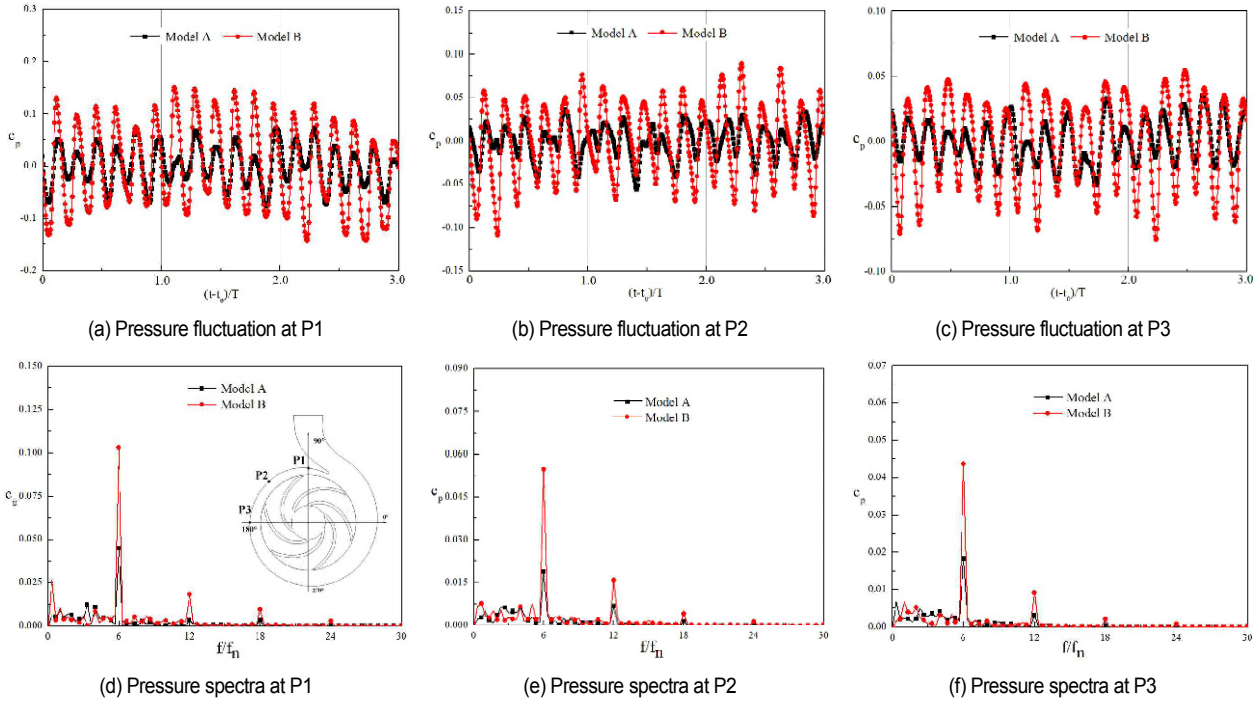

(a) Pressure fluctuation at P1 (b) Pressure fluctuation at P2 (c) Pressure fluctuation at P3

(d) Pressure spectra at P1 (e) Pressure spectra at P2 (f) Pressure spectra at P3

Fig. 11. Pressure fluctuation and frequency spectra at selected monitor points.

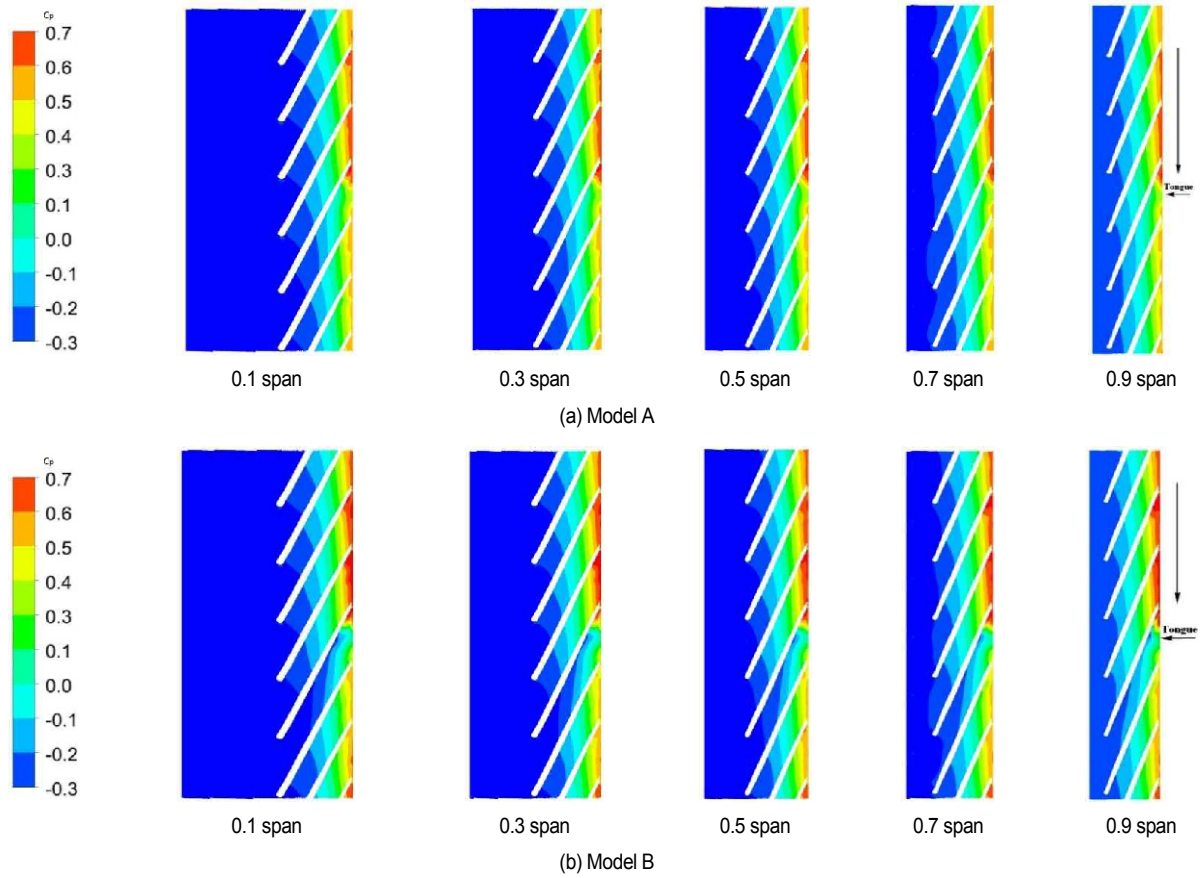

(a) Model A

(b) Model B

Fig. 12. Pressure distribution in blade-to-blade view at different spans.

causes the high-energy flow loss at the impeller outlet, and further reduces the intensity of the pressure fluctuation. As a result, the amplitude of the f_{BPF} of model A is significantly lower than that of model B at the same monitor point. In comparison with model B, the largest amplitude of pressure fluctuation at the monitoring probe from P1, P2, and P3 for model A decreases by 56.38 %, 65.34 %, and 58.36 %, respectively.

Therefore, the internal clearance flow of the centrifugal pump significantly affects the pressure distribution and the pressure fluctuation characteristics. The occurrence of the leakage flow causes the decrease in the pressure, resulting in the energy loss at the impeller outlet and reducing the intensity of the pressure fluctuation inside the pump. Thus, the effect of clearance flow on the pressure distribution of the volute must be considered.

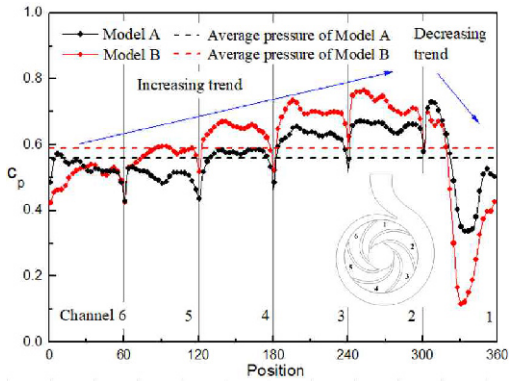

Fig. 13. Pressure distribution on the circumference of the impeller outlet at 0.5 span.

3.3 Effect of clearance flow on pressure distribution of the impeller

Fig. 12 shows the pressure distribution in blade-to-blade view for different spans. As can be seen, the distribution of pressure on the different spans of the two models has a certain similarity. The pressure gradually increases along the flow direction, the minimum value is achieved at the impeller inlet and the maximum value is obtained at the impeller outlet. Meanwhile, the pressure at the inlet of the impeller passage increases along the direction from hub to shroud. However, the difference in the pressure distribution at the impeller outlet is mainly found in the impeller passage directly opposite to the volute tongue for the cases with and without clearance flow. In model A, the pressure distribution in the impeller channels grows gently and is evenly distributed. However, in model B, the pressure distribution in the impeller passage is relatively uneven. The pressure distribution in the flow channel against the tongue is significantly different from that in the other flow channels. The low-pressure area near the pressure side extends along the direction from the inlet to the outlet of the flow channel at different blade-to-blade spans.

Fig. 13 shows the pressure distribution on the circumference of the impeller outlet at 0.5 span and the average pressure is indicated by the dashed line. In general, the pressure on the circumference of the impeller outlet of model A is slightly smaller than that of mode B. The detail deviation of the average pressure at the impeller outlets of model A and model B is 4 %. Along the direction of the impeller rotation, the pressure increases from channel 6 to channel 2. However, in channel 1, the pressure initially decreases and then increases. This phenomenon is more pronounced in model B. In addition, the distribution of pressure on the circumference of the impeller outlet is different for the two models. In model A, the pressure on the circumference of the impeller outlet is relatively uniform. On the contrary, in model B the pressure distribution at impeller outlet is extremely uneven and the pressure fluctuates greatly, especially at the flow channel against the volute tongue. Thus, the influence of the clearance flow on the pressure distribution of the impeller outlet is mainly concentrated at the flow channel against the volute tongue.

Clearance flow significantly affects the pressure distribution inside the impeller. The existence of clearance flow causes the leakage of high-energy fluid at the impeller outlet, which in turn causes the pressure decrease in impeller. The flow channel, which is opposite to the volute tongue, is most affected by clearance flow. In addition, the clearance flow causes the variation of the pressure distribution in the circumferential direction of the impeller outlet.

Fig. 14 shows the pressure coefficient distribution of the blade surface in the impeller passage in the blade-to-blade view at 0.5 span, where L stands for the relative length of the blade. The difference is mainly reflected on the pressure magnitude and distribution on both sides of the flow channel for the cases with and without clearance flow. In general, the pressure magnitude on the pressure side is larger than that on the suction side. This phenomenon results from the energy obtained from the pressure side (PS) of the blade surface. Maximum pressure value is achieved near the region at the outlet of the impeller. The pressure on the suction side (SS) of the blade gradually increases along the direction from the impeller inlet to the impeller outlet. In summary, only a slight difference is observed in pressure on the suction side for the cases with and without clearance flow. The intersections between the pressures of the suction side are observed at approximately 0.6 L. In the area from 0.55 L to 1 L, the pressure distribution on the blade pressure side is quite different. For model A, the pressure magnitude on pressure side increases gently in the area from 0 L to 0.75 L, and then presents rapid growth from 0.7 L to 0.95 L. The pressure decreases at the outlet region of the impeller from 0.95 L to 1.0 L. For model B, a large reduction is found in the pressure magnitude on the pressure side from 0.55 L to 0.70 L. Then, the pressure increases significantly from 0.7 L to 0.95 L. The difference in the pressure distribution indicates that the pressure variation degree on the pressure side of model A is much lower than that of model B.

The relative pressure deviation c_{p1} is adopted to study the pressure distribution on the blade surface to obtain the pres-

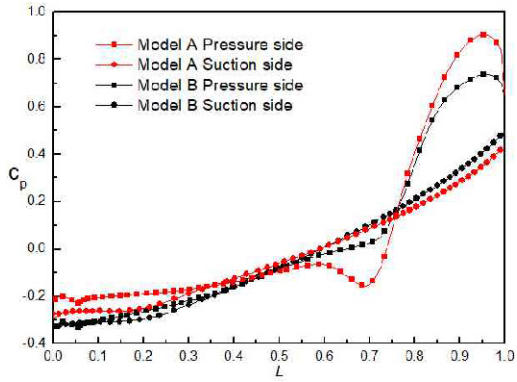

Fig. 14. Pressure distribution on the blade surface at 0.5 span.

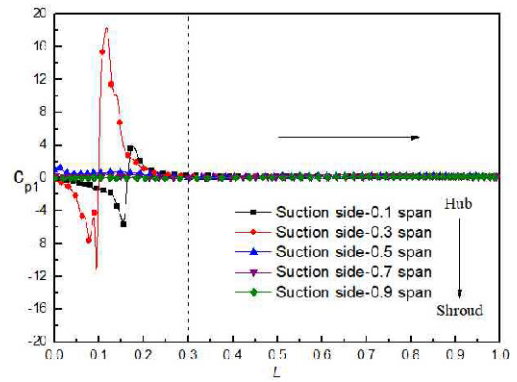

(a) Suction side

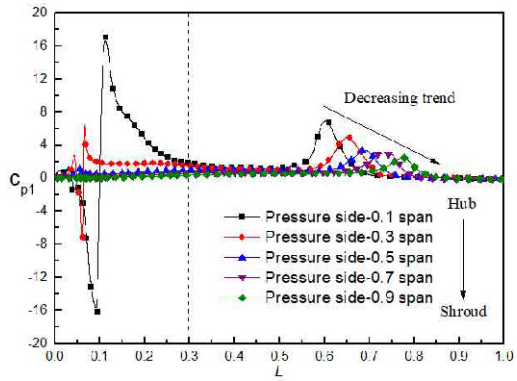

(b) Pressure side

Fig. 15. Distribution of relative pressure deviation on the blade surface.

sure characteristics at different spans on both sides of the flow channel against the volute tongue. The relative pressure deviation c_{p1} is defined as follows:

$$c_{p1} = \frac{p_a - p_b}{p_b} \tag{4}$$

where p_a is the pressure on the blade surface of model A, and p_b is the pressure on the blade surface of model B.

Fig. 15 shows the distribution of the relative pressure deviation c_{p1} on both sides of the flow channel against the tongue. A significant difference is observed in the pressure distribution at the entrance of the impeller (0-0.3 *L*). This phenomenon is mainly caused by the unsteady flow at the leading edge of the impeller blade. From 0.3 *L* to 1.0 *L*, the relative pressure deviation c_{p1} on the suction side (SS) of the blade surface is almost zero for the cases with and without clearance flow, thus indicating the slight difference on the distribution and magnitude of pressure on the suction side of the blade surface, as shown in Fig. 15(a). However, the pressure distribution on the pressure side (PS) is relatively different from that on the suction side. A significant difference in pressure distribution from 0.5 *L* to 0.9 *L* is observed on the pressure side, as shown in Fig. 15(b). In this region, the relative pressure deviation on the pressure side causes the wave distribution, and the peak amplitude decreases in turn along the direction from hub to shroud. This finding that the pressure on the pressure surface of the flow channel is greatly affected by the clearance flow, and the influence is weakened gradually along the direction from hub to shroud.

The clearance flow affects the pressure distribution throughout the impeller, especially in the impeller passage directly facing the volute tongue. The pressure variation in model A is lower than that in model B, which is closely related to the leakage energy loss caused by clearance flow. Therefore, the influence of clearance flow on the pressure distribution in the impeller must be considered for an accurate internal flow distribution.

4. Conclusions

A combined approach of experimental measurement and numerical simulation is used in this study to investigate the performance variation of centrifugal pump with or without clearance flow under low flow rate. The reliability of the numerical results is verified by comparing the external characteristic and the pressure fluctuation experiments. The effect of clearance flow on the internal flow characteristics is analyzed in detail under low flow rate. The main conclusions are summarized below.

(1) Clearance flow significantly reduces the head and efficiency of the centrifugal pump. The average deviations of the head and efficiency under different flow rates are 4.37 % and 19.47 %, respectively, for the cases with and without clearance flow.

(2) The comparative results with or without clearance flow show that the clearance flow causes collision impact with mainstream flow and forms a multiple vortices structure at the impeller entrance.

(3) Clearance flow causes the reduction of pressure inside the pump and results in the decrease in the magnitude and intensity of pressure fluctuation in the volute. The highest amplitude of pressure fluctuation decreased by 65.34 % in the case with clearance flow.

(4) Clearance flow causes the variation of the pressure distribution in the impeller, especially at the flow passage facing

the tongue. The relative pressure deviation on the pressure side, which is affected by the clearance flow, causes wave distribution. In turn, peak amplitude decreases along the hub to shroud direction.

Acknowledgments

This work was financially supported by the Joint Project from the National Natural Science Foundation of China and Zhejiang Province (U1709209), the National Natural Science Foundation of China (51976198, 51579224, 51876103) and the Public Projects of Zhejiang Province (LGG19E060006).

Nomenclature

c_p : Pressure pulsation coefficient (-)
c_{p1} : Relative pressure deviation (-)
b : Wear ring clearance (mm)
D_1 : Inlet diameter of impeller (mm)
D_2 : Outlet diameter of impeller (mm)
D_3 : Inlet diameter of volute (mm)
l : Length of wear ring clearance (mm)
L : Relative length of blade (-)
H : Pump head (m)
H_d : Designed pump head (m)
η : Pump efficiency (%)
n : Rotation speed (r/min)
n_d : Designed rotation speed (r/min)
p : Static pressure (Pa)
p_{ref} : Reference pressure (Pa)
PS : Pressure side (-)
SS : Suction side (-)
TS : Time step (-)
u_2 : Circumferential velocity of impeller
Z : Blade number (-)

References

[1] J. F. Gülich, *Centrifugal Pumps*, Berlin: Springer (2008).
[2] Y. L. Wu, S. C. Li, S. H. Liu, H.-S. Dou and Z. D. Qian, *Vibration of Hydraulic Machinery*, Berlin: Springer (2013).
[3] X. M. Guo, L. H. Zhu, Z. C. Zhu, B. L. Cui and Y. Li, Numerical and experimental investigations on the cavitation characteristics of a high-speed centrifugal pump with a splitter-blade inducer, *Journal of Mechanical Science and Technology*, 29 (1) (2015) 259-267.
[4] X. J. Li, P. L. Gao, Z. C. Zhu and Y. Li, Effect of the blade loading distribution on hydrodynamic performance of a centrifugal pump with cylindrical blades, *Journal of Mechanical Science and Technology*, 32 (3) (2018) 1161-1170.
[5] Y. Li, G. W. Feng, X. J. Li, Q. R. Si and Z. C. Zhu, An experimental study on the cavitation vibration characteristics of a centrifugal pump at normal flow rate, *Journal of Mechanical Science and Technology*, 32 (10) (2018) 4711-4720.
[6] W. X. Ye, R. F. Huang, Z. W. Jiang, X. J. Li, Z. C. Zhu and X. W. Luo, Instability analysis under part-load conditions in centrifugal pump, *Journal of Mechanical Science and Technology*, 33 (1) (2019) 269-278.
[7] R. Spence and J. Amaral-Teixeira, A CFD parametric study of geometrical variations on the pressure pulsations and performance characteristics of a centrifugal pump, *Computers & Fluids*, 38 (6) (2009) 1243-1257.
[8] L. L. Zheng, H.-S. Dou, X. P. Chen, Z. C. Zhu and B. L. Cui, Pressure fluctuation generated by the interaction of blade and tongue, *Journal of Thermal Science*, 27 (1) (2018) 8-16.
[9] J. J. Feng, F.-K. Benra and H. J. Dohmen, Investigation of periodically unsteady flow in a radial pump by CFD simulations and LDV measurements, *Journal of Turbomachinery*, 133 (1) (2011) 011004.
[10] W. Z. Zhang, Z. Y. Yu and B. S. Zhu, Influence of tip clearance on pressure fluctuation in low specific speed mixed-flow pump passage, *Energies*, 10 (2) (2017) 148.
[11] J. S. Zhang and L. Tan, Energy performance and pressure fluctuation of a multiphase pump with different gas volume fractions, *Energies*, 11 (5) (2018) 1216.
[12] Z. F. Yao, F. J. Wang, L. X. Qu, R. F. Xiao, C. L. He and M. Wang, Experimental investigation of time-frequency characteristics of pressure fluctuations in a double-suction centrifugal pump, *ASME Journal of Fluids Engineering*, 133 (10) (2011) 101303.
[13] B. Gao, N. Zhang, Z. Li, D. Ni and M. G. Yang, Influence of the blade trailing edge profile on the performance and unsteady pressure pulsations in a low specific speed centrifugal pump, *ASME Journal of Fluids Engineering*, 138 (5) (2016) 051106.
[14] B. Gao, P. M. Guo, N. Zhang, Z. Li and M. G. Yang, Unsteady pressure pulsation measurements and analysis of a low specific speed centrifugal pump, *ASME Journal of Fluids Engineering*, 139 (7) (2017) 071101.
[15] R. Spence and J. Amaral-Teixeira, Investigation into pressure pulsations in a centrifugal pump using numerical methods supported by industrial test, *Computers & Fluids*, 37 (6) (2008) 690-704.
[16] N. Zhang, M. G. Yang, B. Gao, L. Zhong and N, Dan, Experimental investigation on unsteady pressure pulsation in a centrifugal pump with special slope volute, *ASME Journal of Fluids Engineering*, 137 (6) (2015) 061103.
[17] L. L. Zheng, H.-S. Dou, X. P. Chen, Z. C Zhu and B. L. Cui, Numerical investigation of flow instability in centrifugal pump based on energy gradient method, *ASME Turbo Expo 2016: Turbomachinery Technical Conference and Exposition*, Seoul (2016) V02DT44A032.
[18] X. P. Chen, Z. C. Zhu, H.-S. Dou and L. Yi, Large eddy simulation of energy gradient field in a centrifugal pump impeller, *Proceedings of the Institution of Mechanical Engineers, Part C: Journal of Mechanical Engineering Science*, 233 (11) (2019) 4047-4057.
[19] T. Sano, Y. Yoshida, Y. Tsujimoto, Y. Nakamura and T. Matsushima, Numerical study of rotating stall in a pump vaned diffuser, *ASME Journal of Fluids Engineering*, 124 (2) (2002) 363-370.
[20] O. Pacot, C. Kato, Y. Guo, Y. Yamade and F. Avellan, Large

eddy simulation of the rotating stall in a pump-turbine operated in pumping mode at a part-load condition, *ASME Journal of Fluids Engineering*, 138 (11) (2016) 111102.

[21] A. Lucius and G. Brenner, Numerical simulation and evaluation of velocity fluctuations during rotating stall of a centrifugal pump, *ASME Journal of Fluids Engineering*, 133 (8) (2011) 081102.

[22] M. Sinha, A. Pinarbasi and J. Katz, The flow structure during onset and developed states of rotating stall within a vaned diffuser of a centrifugal pump, *ASME Journal of Fluids Engineering*, 123 (3) (2001) 490-499.

[23] K. Brun and R. Kurz, Analysis of secondary flows in centrifugal impellers, *International Journal of Rotating Machinery*, 2005 (1) (2005) 45-52.

[24] Z. Zhang, Rotating stall mechanism and stability control in the pump flows, *Proceedings of the Institution of Mechanical Engineers, Part A: Journal of Power and Energy*, 225 (6) (2011) 779-788.

[25] J. Gonzalez, J. Fernández, E. Blanco and C. Santolaria, Numerical simulation of the dynamic effects due to impeller-volute interaction in a centrifugal pump, *ASME Journal of Fluids Engineering*, 124 (2) (2002) 348-355.

[26] R. W. Westra, L. Broersma, K. van Andel and N. P. Kruyt, PIV measurements and CFD computations of secondary flow in a centrifugal pump impeller, *ASME Journal of Fluids Engineering*, 132 (6) (2010) 061104.

[27] L. Cao, Y. X. Xiao, Z. W. Wang, Y. Y. Luo and X. R. Zhao, Pressure fluctuation characteristics in the sidewall gaps of a centrifugal dredging pump, *Engineering Computations*, 34 (4) (2017) 1054-1069.

[28] D. S. Zhang, W. D. Shi, B. P. M. B. Van Esch, L. Shi and M. Dubuisson, Numerical and experimental investigation of tip leakage vortex trajectory and dynamics in an axial flow pump, *Computers & Fluids*, 112 (2) (2015) 61-71.

[29] D. S. Zhang, W. D. Shi, D. Z. Pan and M. Dubuisson, Numerical and experimental investigation of tip leakage vortex cavitation patterns and mechanisms in an axial flow pump, *ASME Journal of Fluids Engineering*, 137 (12) (2015) 121103.

[30] B. C. Will, F. K. Benra and H. J. Dohmen, Investigation of the flow in the impeller side clearances of a centrifugal pump with volute casing, *Journal of Thermal Science*, 21 (3) (2012) 197-208.

[31] X. Q. Jia, B. L. Cui, Y. L. Zhang and Z. C. Zhu, Study on internal flow and external performance of a semi-open impeller centrifugal pump with different tip clearances, *International Journal of Turbo & Jet-Engines*, 32 (1) (2015) 1-12.

[32] J. J. Feng, X. Q. Luo, P. C. Guo and G. K. Wu, Influence of tip clearance on pressure fluctuations in an axial flow pump, *Journal of Mechanical Science and Technology*, 30 (4) (2016) 1603-1610.

[33] X. L. Fu, D. Y. Li, H. J. Wang, G. H. Zhang, Z. G. Li and X. Z. Wei, Influence of the clearance flow on the load rejection process in a pump-turbine, *Renewable Energy*, 127 (2018) 310-321.

[34] Y. B. Liu and L. Tan, Spatial-temporal evolution of tip leakage vortex in a mixed-flow pump with tip clearance, *ASME Journal of Fluids Engineering*, 141 (8) (2019) 081302.

[35] L. Cao, Y. Y. Zhang, Z. W. Wang, Y. X. Xiao and R. X. Liu, Effect of axial clearance on the efficiency of a shrouded centrifugal pump, *ASME Journal of Fluids Engineering*, 137 (7) (2015) 071101.

[36] H. L. Liu, J. Ding, H. W. Dai and M. G. Tan, Investigation into transient flow in a centrifugal pump with wear ring clearance variation, *Advances in Mechanical Engineering*, 6 (2014) 693097.

[37] W. G. Zhao, M. Y. He, C. X. Qi and Y. B. Li, Research on the effect of wear-ring clearances to the axial and radial force of a centrifugal pump, *IOP Conference Series: Materials Science and Engineering*, 52 (2013) 072015.

[38] W. G. Li, An experimental study on the effect of oil viscosity and wear-ring clearance on the performance of an industrial centrifugal pump, *ASME Journal of Fluids Engineering*, 134 (1) (2012) 014501.

[39] M. DaqiqShirazi, R. Torabi, A. Riasi and S. A. Nourbakhsh, The effect of wear ring clearance on flow field in the impeller sidewall gap and efficiency of a low specific speed centrifugal pump, *Proceedings of the Institution of Mechanical Engineers, Part C: Journal of Mechanical Engineering Science*, 232 (17) (2018) 3062-3073.

[40] J. R. Yan, Z. T. Zuo, W. B. Guo, H. C. Hou, X. Zhou and H. S. Chen, Influences of wear-ring clearance leakage on performance of a small-scale pump-turbine, *Proceedings of the Institution of Mechanical Engineers, Part A: Journal of Power and Energy* (2019).

[41] K. Majidi, Numerical study of unsteady flow in a centrifugal pump, *ASME Journal of Turbomachinery*, 127 (2) (2005) 363-371.

[42] L. Zhou, W. D. Shi, W. Li and R. Agarwal, Numerical and experimental study of axial force and hydraulic performance in a deep-well centrifugal pump with different impeller rear shroud radius, *ASME Journal of Fluids Engineering*, 135 (10) (2013) 104501.

[43] Y. X. Fu, J. P. Yuan, S Q. Yuan, G. Pace, L. d'Agostino, P. Huang and X. J. Li, Numerical and experimental analysis of flow phenomena in a centrifugal pump operating under low flow rates, *ASME Journal of Fluids Engineering*, 137 (1) (2015) 011102.

[44] Z. X. Gao, W. R Zhu, L. Lu, J. Deng, J. G. Zhang and F. J. Wuang, Numerical and experimental study of unsteady flow in a large centrifugal pump with stay vanes, *ASME Journal of Fluids Engineering*, 136 (7) (2014) 071101.

[45] S. S Yang, H. L. Liu, F. Y. Kong, B. Xia and L. W. Tan, Effects of the radial gap between impeller tips and volute tongue influencing the performance and pressure pulsations of pump as turbine, *ASME Journal of Fluids Engineering*, 136 (5) (2014) 054501.

[46] B. Gao, N. Zhang, Z. Li, D. Ni and M. G. Yang, Influence of the blade trailing edge profile on the performance and unsteady pressure pulsations in a low specific speed centrifugal pump, *ASME Journal of Fluids Engineering*, 138 (5) (2016) 051106.

[47] B. Gao, P. M. Guo, N. Zhang, Z. Li and M. G. Yang, Unsteady

pressure pulsation measurements and analysis of a low specific speed centrifugal pump, *ASME Journal of Fluids Engineering*, 139 (7) (2017) 071101.

[48] Q. R. Si, J. P. Yuan, S. Q. Yuan, W. J. Wang, L. Zhu and G. Bois, Numerical investigation of pressure fluctuation in centrifugal pump volute based on SAS model and experimental validation, *Advances in Mechanical Engineering*, 6 (2014) 972081.

Lulu Zheng is currently a lecturer at Henan Institute of Technology, China. He received his Ph.D. degree from Zhejiang Sci-Tech University in 2018. His main areas of interest are turbomachinery, clearance flow and computational fluid dynamics.